

## ELECTROOSMOTIC PUMPS FABRICATED FROM POROUS SILICON MEMBRANES

Shuhuai Yao<sup>1</sup>, Alan M. Myers<sup>2</sup>, Jonathan D. Posner<sup>1</sup>, and Juan G. Santiago<sup>1</sup>  
<sup>1</sup>Department of Mechanical Engineering, Stanford University, Stanford, CA 94305  
<sup>2</sup>Intel Corporation

### ABSTRACT

Large flow rates per applied potential are obtained from electroosmotic (EO) pumps fabricated from n-type porous silicon. Porous silicon membranes have ideal geometries for EO pumping. These membranes have hexagonally packed, uniform pores with near-unity tortuosity and are well suited to maximize flow rate for a given applied voltage. The 350  $\mu\text{m}$  thick membranes were passivated with a  $\text{SiO}_2$  layer and exhibit a maximum flow rate of 1.2 ml/min/cm<sup>2</sup>/V. This is 4.4 times higher than previously demonstrated silica-based frit EO pumps. LPCVD polysilicon deposition followed by wet oxidation was used to control the pore size. The impact of these coatings on the pump performance has also been characterized.

### INTRODUCTION

EO pumps have no moving parts and are capable of generating both high flow rate and significant pressure capacity with a compact device volume and using tens to hundreds of volts. They therefore offer advantages over other miniature pumps for microchannel cooling applications [1]. Packed-column EO pumps have been fabricated by packing and sintering 1-20  $\mu\text{m}$  silica and borosilicate glass particles [2-8]. In parallel efforts, Chen and Santiago [9] and Laser et al. [10] demonstrated EO pumps fabricated using planar micromachined structures in glass and silicon substrates. EO pumps have also been fabricated using commercially available porous glass frits (e.g., from Robu Glasfilter-Geräte GmbH, Germany). These glass filters, or "frits", are 40 mm in diameter, 1-5 mm thick, with mean pore diameters of 1 to 2  $\mu\text{m}$ , porosities of 0.2 to 0.35, and tortuosities of 1.4. The minimum power requirement of such pumps is limited by the morphology (tortuosity), the ability to reproducibly fabricate submicron pore diameters, and structural strength [11]. Laser and Santiago [12] present comparisons of EO pumps to other miniature pump technologies.

Porous silicon has attracted increasing interest in a wide spectrum of potential applications [13, 14]. A porous silicon membrane consists of a dense array of straight pores. Pores are nearly uniform in characteristic diameter and are advantageous over pores in silica-based frits as they have a tortuosity

approaching unity. We have modeled EO pumping in porous materials by treating the media as an array of cylindrical microchannels of uniform pore radius,  $a$ , with tortuosity,  $\tau$ , and porosity,  $\psi$ . Flow rate dependence on applied potential and pressure can then be described as [15]:

$$Q = \psi \left[ \frac{PAa^2}{8\mu L} - \frac{\varepsilon\zeta AV}{\mu L} f \right] \quad (1)$$

where  $f = \int_0^a \left( 1 - \frac{\phi}{\zeta} \right) \frac{2r}{a^2} dr$  (2)

The solution to the integral can be obtained by solving the Poisson-Boltzmann equation for electrical potential in the channel [15, 16]. Silicon microfabrication techniques offer excellent control of porous structure thickness, pore radius, and porosity. The ratio of the maximum flow rate to the maximum achievable pressure of an EO pump,  $Q_{max}/P_{max}$ , can be expressed as:

$$Q_{max}/P_{max} = \psi A a^2 / (8\mu L) \quad (3)$$

This paper presents a description of the fabrication and characterization of EO pumps fabricated using porous silicon membranes. Silicon structures have been modified with a suitable thin film deposition including thermal oxide, LPCVD nitride, or oxidized LPCVD polysilicon to provide reliable insulation surfaces. The effects of pore size and porosity on flow rate and pressure have been demonstrated by eight samples with various polysilicon deposition thicknesses and analyzed based on a theoretical model. The repeatability and stability of pump operation has also been studied for choice of working solutions.

### NOMENCLATURE

$A$	Cross-sectional area
$L$	Length
$I$	Current
$P$	Pressure capacity
$Q$	Flow rate
$V$	Potential
$a$	Pore radius
$d$	Center-to-center distance
$\varepsilon$	Permittivity of liquid

$\mu$	Viscosity
$\zeta$	Zeta potential
$\psi$	Porosity
$\tau$	Tortuosity

## MATERIALS AND FABRICATION

The porous silicon structures used here were fabricated from n-type silicon by Neah Power Systems, Inc. (Bothell, WA). These 350  $\mu\text{m}$  thick membranes have a hexagonal array of uniform pores with a tortuosity approaching unity. The porosity is determined by the hexagon layout and feature dimensions as follows

$$\psi = 2\pi a^2 / (\sqrt{3}d^2) \quad (4)$$

where  $a$  is the pore diameter and  $d$  is the center-to-center distance of pores. Fig. 1 shows scanning electron microscope (SEM) images of the top and cross-sectional view of porous silicon membranes. The top view shows the membrane's hexagonal array of pores with diameters on the order of 5  $\mu\text{m}$  and center-to-center distances of 8  $\mu\text{m}$ . The porosity of these structures is 0.35. The cross-sectional SEM shows straight pores.

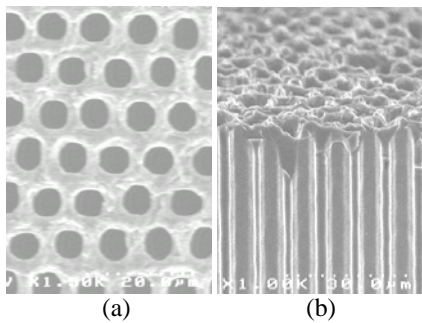


**Figure 1.** SEM of porous silicon structure. The sample (obtained from Neah Power Systems, Inc. Bothell, WA) is coated with a  $\text{SiO}_2$  thin film. (a) Top view showing a hexagonal array of pores with diameters on the order of 5  $\mu\text{m}$  and pitch distances of 8  $\mu\text{m}$ . (b) Cross-sectional view showing straight pores with a uniform, conformal coating approximately 0.25  $\mu\text{m}$  thick.

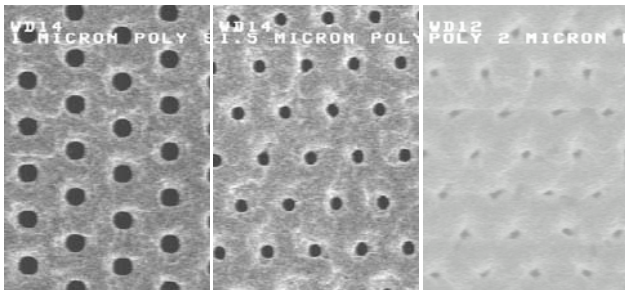


**Figure 2.** Top view SEMs of porous silicon structures with polysilicon deposition thickness of 1  $\mu\text{m}$ , 1.5  $\mu\text{m}$  and 2  $\mu\text{m}$ . These polysilicon layers were wet oxidized to have 0.25  $\mu\text{m}$   $\text{SiO}_2$  coating surfaces.

The silicon structures were modified with a suitable thin film deposition including thermal oxide, LPCVD nitride, or oxidized LPCVD polysilicon. The liner materials on the silicon substrate provide reliable insulation for operation. The  $\text{SiO}_2$  coating also improves surface charge density and operating stability of the pump. LPCVD polysilicon deposition, followed by wet oxidation of the polysilicon layer, is used to increase the coating thickness, and provide better control of pore diameter. In this study, we have tried LPCVD polysilicon deposition for 0.3 to 2.5 hr, resulting in polysilicon deposition thickness varying from 0.25 to 2  $\mu\text{m}$  (Table 1). Fig. 2 shows top down view SEMs of the porous silicon structures with polysilicon deposition thickness of 1  $\mu\text{m}$ , 1.5  $\mu\text{m}$  and 2  $\mu\text{m}$ .

## EXPERIMENTAL SETUP

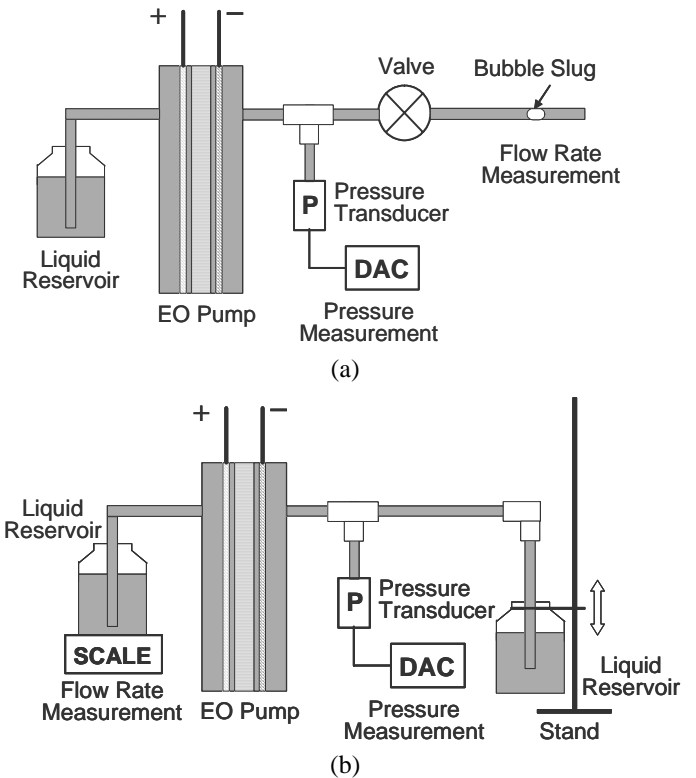


**Figure 3.** (a) Schematic of test setup for pump characterization. A control valve is used to set desired pressure loads. Flow rate, current and back pressure are measured. (b) Schematic of setup with extended capability for varying back pressure. The back pressure is changed by varying the height of the hydraulic head along the stand.

The experimental setup for characterizing pump performance is shown in Fig. 3a. A Kepco power supply (Kepco Inc., Flushing, NY) provides electric field across the electrodes of the pump. A micro-metering control valve (Upchurch Scientific, Oak Harbor, WA) downstream of the pump is used to set desired pressure loads. Flow rate is measured by monitoring the motion of electrolytic bubble "slugs" in the output line of the pump. Pressure is measured downstream of the pump using a pressure transducer (OMEGA, Stamford, CT). The pressure and current signals are recorded

using an automated data acquisition system (Agilent, Palo Alto, CA). The porous silicon structures are cleaned using 100 mM NaOH and rinsed with deionized water. The structures are then cleaned in an ultrasonic bath (Fisher Scientific, Hanover Park, IL) with deionized water for 20 min. The working electrolyte in these experiments was 1 mM ( $\text{Na}^+$ ) borate buffer solutions ( $\text{Na}_2\text{B}_4\text{O}_7$ ) with conductivity 80  $\mu\text{S}/\text{cm}$  and pH 9.2. Conductivity and pH were measured using a dual conductivity and pH meter (Cole-Parmer Instrument, Vernon Hills, IL).

A second setup with extended capability for varying back pressure (Fig 3b) allows for the measurement of the full pressure capacity of the pump in flowing conditions. This setup allows for the measurement of EO pumping under adverse pressures higher than the maximum pressure of the pump and under negative load pressure (i.e., favorable pressure gradient in the pores). The back pressure is varied by changing the hydraulic head along the stand. The flow rate is measured using a balance (ACCULAB, Newtown, PA) upstream of the pump. This approach provides a more stable, repeatable method to measure the pump performance.

## RESULTS AND DISCUSSION

First, the dielectric breakdown strength of the porous-silicon-based EO pumps was determined for an oxide/porous-silicon sample. The porous silicon membrane was wet oxidized at 900 °C for 2 hr with an accompanying 10 min dry oxidation both preceding and following the wet oxidation. The estimated oxide film thickness is 0.25  $\mu\text{m}$ . The data of Fig. 4 demonstrates that the  $\text{SiO}_2$  coating provides reliable insulation for operation at up to approximately 400 V (the data point labeled with an “x” is the first current measurement immediately after breakdown). Before breakdown, the electric current is proportional to the applied voltage and the resistance is relatively high. In a subsequent experiment performed after breakdown, the system resistance is reduced by a factor of 2.5 and current shows a slightly nonlinear increase with the voltage.

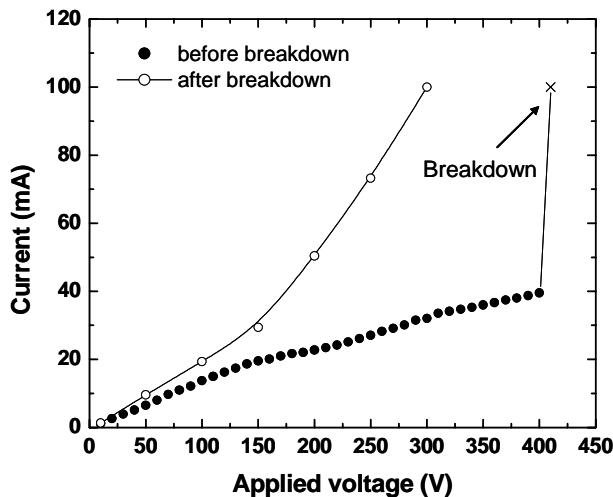


**Figure 4.** Porous silicon EO pump current versus applied voltage at 10 V intervals to 410 V (dark symbols). Electrical breakdown occurred between 400 and 410 V. Before breakdown, the electric current is proportional to the applied voltage and the resistance is relatively high. After breakdown (open symbols), the system resistance is reduced by a factor of 2.5.

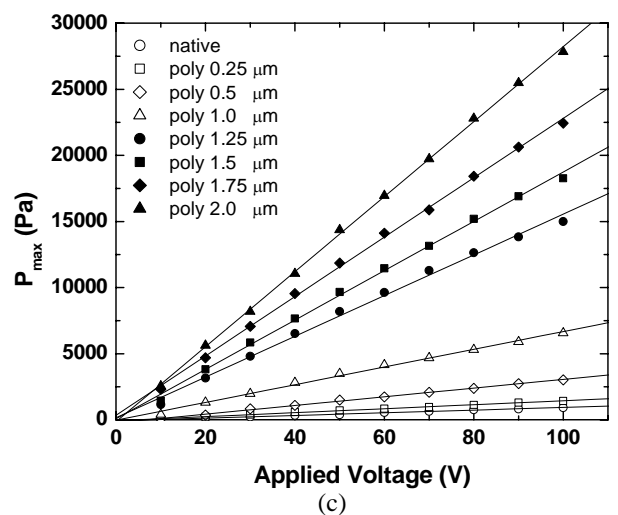
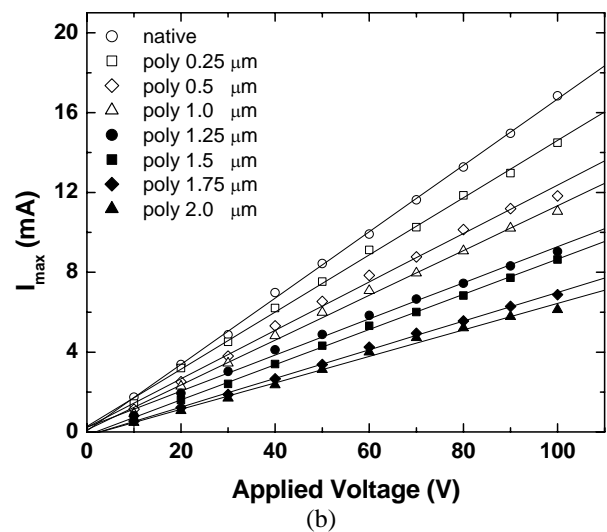
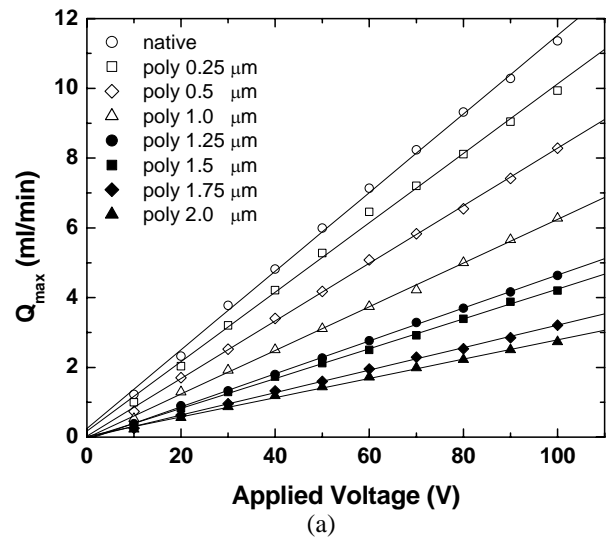


**Figure 5.** Maximum flow rate, current, and pressure versus applied voltage for porous silicon EO pumps with various thicknesses of polysilicon deposition and 0.25  $\mu\text{m}$  thick  $\text{SiO}_2$  surface layers.

**Table 1.** Pore radius estimated from fabrication process (Fab.) and flow performance ( $Q_{max}/P_{max}$ ) and associated porosity estimations

	$a$ ( $\mu\text{m}$ )		$\psi$	
	Fab.	$Q_{max}/P_{max}$	Fab.	$Q_{max}/P_{max}$
Native SiO <sub>2</sub>	2.5	2.73	0.35	0.42
0.25 $\mu\text{m}$ poly + SiO <sub>2</sub>	2	2.56	0.23	0.37
0.5 $\mu\text{m}$ poly + SiO <sub>2</sub>	1.75	2.04	0.17	0.24
1.0 $\mu\text{m}$ poly + SiO <sub>2</sub>	1.25	1.73	0.09	0.17
1.25 $\mu\text{m}$ poly + SiO <sub>2</sub>	1	1.18	0.06	0.08
1.5 $\mu\text{m}$ poly + SiO <sub>2</sub>	0.75	1.12	0.03	0.07
1.75 $\mu\text{m}$ poly + SiO <sub>2</sub>	0.5	1.01	0.014	0.06
2.0 $\mu\text{m}$ poly + SiO <sub>2</sub>	0.25	0.86	0.004	0.04

Eight porous silicon membranes were tested in this study. One of these had a native oxide surface and the rest had various thicknesses of polysilicon deposition followed by wet oxidation. Table 1 summarizes the characterization data of these membranes. The pore radius is estimated from the fabrication process as well as from Eq. (3) with a measurement of  $Q_{max}/P_{max}$ . Porosity in both cases is calculated using Eq. (4). Fig. 5 shows a linear dependence of maximum pump flow rate,  $Q_{max}$ , maximum pump current,  $I_{max}$ , and maximum pump pressure,  $P_{max}$  with applied voltage for these porous silicon EO pumps [12]. The largest flow rate pump was the membrane with native SiO<sub>2</sub>, as expected (note that all membranes had an equal number density of pores). The thickness of this native oxide was less than 20 Å. The pore radius of this native oxide pump was approximately 2.5  $\mu\text{m}$  and the porosity 0.35. The flow rate per unit applied voltage and unit area was 1.2 ml/min/cm<sup>2</sup>/V. The highest measured pressure per unit applied voltage was 345 Pa/V, achieved by the membrane with 2  $\mu\text{m}$  polysilicon deposition and 0.25  $\mu\text{m}$  SiO<sub>2</sub> coating surfaces. The zeta potential of these porous silicon membranes is estimated as -104 mV by the methods described in our previous paper [11]. This value is comparable to the zeta potential of -106 mV value for borosilicate glass operated with the same buffered electrolyte [11]. Because the charge sites on SiO<sub>2</sub> are invariably Si-OH, regardless of the silica type or deposition technique, thin SiO<sub>2</sub> layers perform much like bulk silica [17]. The highest measured thermodynamic efficiency for these pumps was 0.2 %, the same value as measured with borosilicate pumps with the same buffered electrolyte [11].

Figure 6a shows the characterization of pump performance with various thicknesses of polysilicon deposition and 0.25  $\mu\text{m}$  SiO<sub>2</sub> coating surfaces at 25 V applied potential. The flow rate and pressure were measured at steady state conditions. The analytical expression of Eqs. (3) and (4) can be used to estimate the pore radius. The results are compared with the nominal values from fabrication process, as shown in Table 1. Fig. 6b shows the normalized flow rate versus pressure. The flow rate and pressure are non-dimensionalized by  $-\psi A \epsilon \zeta V / (\mu L)$  and  $-8 \epsilon \zeta V / a^2$ , using a value of -104 mV for the zeta potential. The data in these coordinates should collapse onto a single line, yet there is a clear discrepancy in the absolute values of maximum normalized flow rate and pressure (although nearly equal slopes). We attribute this unexpected scaling to the fact that many of the pores in the samples were in fact not opened during the fabrication process. We have partially confirmed

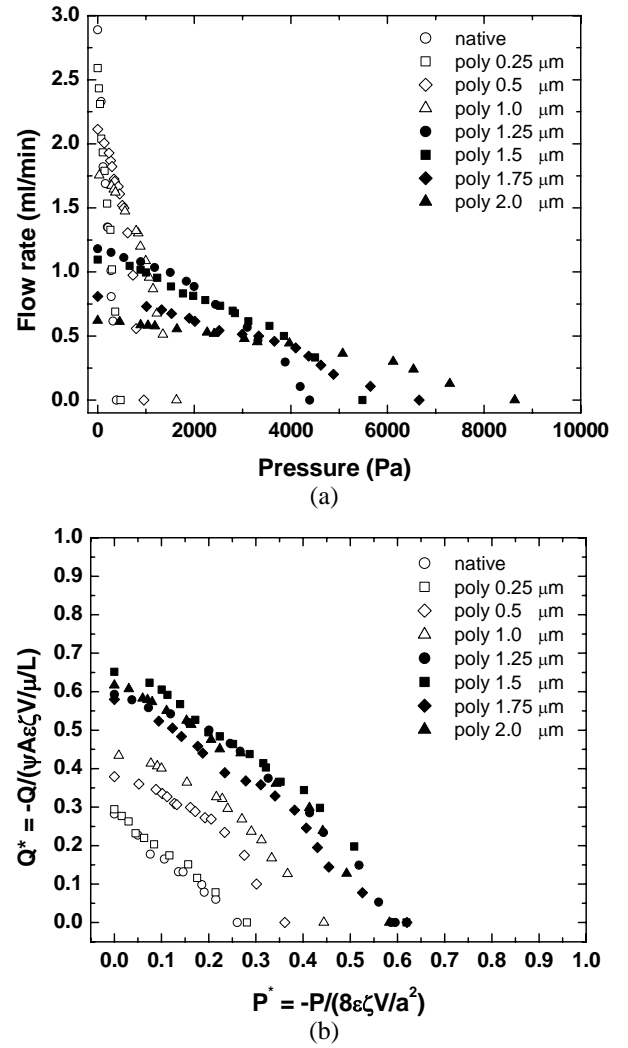


**Figure 6.** (a) Flow rate versus backpressure for porous silicon EO pumps with various thicknesses of polysilicon deposition and 0.25  $\mu\text{m}$  SiO<sub>2</sub> coating surfaces at an applied potential of 25 V. (b) Normalized flow rate vs. pressure.

this hypothesis using a few SEMs and optical images of the membranes (which clearly show that a fraction of the pores are closed). In a future paper, we will use measured values of pore numbers and pore diameters to normalize data and more accurately characterize these pumps.

The flow rate-pressure results presented above were repeatable to within  $\pm 11$  % over multiple realizations performed with the same pump. Fig. 7a shows flow rate versus backpressure data for the porous silicon pump with 1.25  $\mu\text{m}$  polysilicon deposition and 0.25  $\mu\text{m}$  SiO<sub>2</sub> coating surfaces at 25 V applied potential. Shown are results for six realizations. The curves are roughly linear throughout much of the flow rate and pressure range, as predicted by Eq. (1), but the flow rate and pressure were lower than expected at low flow conditions. We attribute this behavior at high pressures to unwanted gradients in pH. At high pressure/low flow conditions, there is less transport of buffer through the pump and electrolytic current can overcome the buffering strength of the buffer. This

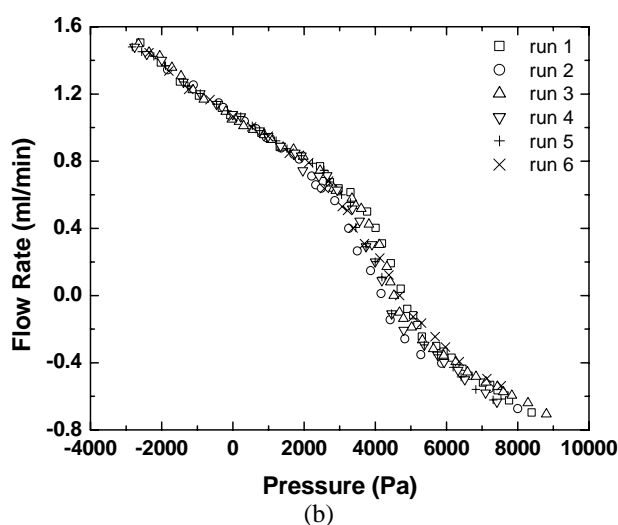
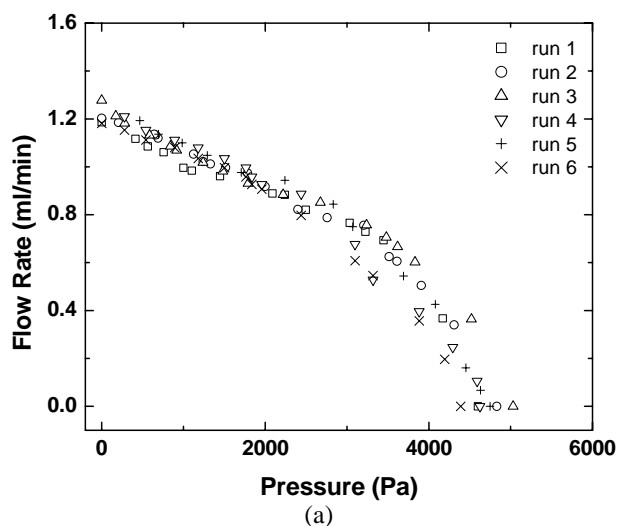


**Figure 7.** (a) Flow rate versus backpressure for the porous silicon pump with 1.25  $\mu\text{m}$  polysilicon deposition and 0.25  $\mu\text{m}$   $\text{SiO}_2$  coating surfaces at applied potential of 25 V the setup of Fig. 3a. (b) Flow rate versus backpressure data from favorable pressure differences to adverse pressure loads in excess of pump pressure capacity using the setup of Fig. 3b. Shown are data from six realizations demonstrating repeatability of the process.

creates a condition where the pH of the upstream electrolyte (at the anode) decreases and this adversely impacts the zeta potential and pump performance. This hypothesis was confirmed using visualizations performed with a universal pH indicator solute (Sigma-Aldrich, Allentown, PA), which showed upstream electrolyte regions of pH below about 8 at low flow conditions.

We further tested the performance of pumps using the setup shown in Fig. 3b. We varied the hydraulic head of the downstream liquid reservoir to impose a net reverse flow opposing the action of the pump. Extended pressure and flow rate data are shown in Fig. 7b for six realizations with the same pump. At high flow conditions (above 0.4 ml/min and below -0.4 ml/min), pressure-flow rate slopes are nearly equal. However, both pressure and flow rate noticeably drop to lower

values at low flow conditions (again due to unfavorable pH conditions at the low flow rate condition). Steady-state pumping performance was observed for 1 hr of operation in each realization. The maximum flow rate and current were  $1 \pm 0.07$  ml/min and  $2.42 \pm 0.14$  mA, respectively. The stability of flow performance needs to be further investigated by long-term experiments. As zeta potential is a function of both pH and ion density, buffer selection is essential to the stable operation of any EO pump [4]. We suggest electrolyte chemistry be chosen as a trade-off between flow capacity (per unit area and electric field) and operational stability.

## CONCLUSION AND FUTURE WORK

We have demonstrated EO pumping of large flow rate per unit potential and area using porous silicon structures as the pumping media. Our prototyped porous silicon pumps generate a maximum flow rate of 2.9 ml/min at 25 V applied voltage with a compact pumping medium volume of 35  $\text{mm}^3$ . The geometry and material of the pumping structures are characterized in the terms of porosity and pore size. We are currently applying image analysis techniques to optical micrographs and the scanning electron micrographs in an effort to directly measure pore number density and pore diameter. This should provide more insight in investigations of the effects of coating thickness on the pumping performance. We are also investigating porous silicon membranes with higher pore density and porosity to optimize both the flow rate and pressure performance of these pumps.

## ACKNOWLEDGMENTS

This work is supported by Intel Corporation. Work was performed in part at the Stanford Nanofabrication Facility (a member of the National Nanotechnology Infrastructure Network) which is supported by the National Science Foundation under Grant ECS-9731294. We would also like to thank Neah Power Systems for providing the porous silicon membranes.

## REFERENCES

- [1] Jiang, L., Mikkelsen J. C., Koo, J.-M., Huber, D., Yao, S., Zhang, L., Zhou, P., Maveety J. G., Prasher R., Santiago J. G., Kenny T. W., and Goodson K. E., 2002, "Closed-loop electroosmotic microchannel cooling system for VLSI circuits," IEEE Transactions on Components & Packaging Technologies, **25**(#3), pp.347-355.
- [2] Proetorius, V., Hopkins, B. J., and Schieke, J. D., 1974, "Electroosmosis: a new concept for high-speed liquid chromatography," Journal of Chromatography A, **99**, pp. 23-30.
- [3] Theeuwes F., 1975, "Elementary osmotic pump," Journal of Pharmaceutical Sciences, **64**(#12), pp. 1987-1991.
- [4] Gan, W., Yang, L., He, Y., Zeng, R., Cervera, M. L., and Guardia M. de la, 2000, "Mechanism of porous core electroosmotic pump flow infection system and its application to determination of chromium (VI) in waste-water," Talanta, **51**, pp. 667-675.

- [5] Paul, P. H., and Rakestraw, D.J., 2000, "Electrokinetic high pressure hydraulic system," U.S. Patent, No. 6,019,882.
- [6] Zeng, S., Chen, C. H., Santiago, J. G., Chen, J., Zare, R. N., Tripp, J. A., Svec, F., and Fréchet. J., 2001, "Electroosmotic flow pumps with polymer frits," *Sensors and Actuators B*, **82**(#2-3), pp. 209-212.
- [7] Zeng, S., Chen, C. H., Mikkelsen, J. C., and Santiago, J. G., 2001, "Fabrication and characterization of electroosmotic micropumps," *Sensors and Actuators B*, **79** (#2-3), pp. 107-114.
- [8] Yao, S., Huber, D., Mikkelsen, J. C., and Santiago, J. G., 2001, "A large flowrate electroosmotic pump with micron pores," Proceedings of the International Mechanical Engineering Congress and Exposition, Sixth Microfluidics Symposium, New York, New York.
- [9] Chen, C. H., and Santiago, J.G., 2002, "A planar electroosmotic micropump," *Journal of Microelectromechanical Systems*, **11**(#6), pp. 672-683.
- [10] Laser, D. J., Yao, S., Chen, C. H., Mikkelsen, J. C., Goodson K. E., Santiago, J.G., and Kenny T. W., 2001, "A low-voltage silicon micromachined parallel-plate electrokinetic pump," Proceedings of the 11th International Conference on Solid-State Sensors and Actuators (Transducers '01), Munich, Germany.
- [11] Yao, S., Hertzog, D. E., Zeng, S., Mikkelsen, J. C., and Santiago, J. G., 2003, "Porous glass electroosmotic pumps: design and experiments," *Journal of Colloid Interface Science*, **268**, pp.143-153.
- [12] Laser, D. J., and Santiago, J. G., 2004, "A review of micropumps," *Journal of Micromechanics and Microengineering*, **14**(#6), pp. R35-64.
- [13] Föll, H., Christophersen, M., Carstensen, J., and Hasse, G., 2002, "Formation and application of porous silicon," *Materials Science and Engineering R*, **39**, pp. 93-141.
- [14] Presting, H., Konle, J., Starkov, V., Vyatkin, A., and Konig, U., 2004, "Porous silicon for micro-sized fuel cell reformer units," *Materials Science and Engineering B*, **108**(#1-2), pp.162-165.
- [15] Yao, S., and Santiago, J. G., 2003, "Porous glass electroosmotic pumps: theory," *Journal of Colloid Interface Science*, **268**, pp.133-142.
- [16] Hunter, R. J., 1981, *Zeta Potential in Colloidal Science: Principles and Applications*, Academic Press, London.
- [17] Kirby, B.J., and Hasselbrink, E.F. Jr., 2004, "The zeta potential of microfluidic substrates. 1. Theory, experimental techniques, and effects on separations," *Electrophoresis*, **25**(#2), pp.187-202.